



Non-linear processing with a surface acoustic wave reservoir computer

Claude Meffan¹ · Taiki Ijima¹ · Amit Banerjee¹ · Jun Hirotsu¹ · Toshiyuki Tsuchiya¹

Received: 31 December 2022 / Accepted: 24 April 2023 / Published online: 17 May 2023
© The Author(s), under exclusive licence to Springer-Verlag GmbH Germany, part of Springer Nature 2023

Abstract

Reservoir computing is a neural network algorithm that reduces the training needed for a neural network to be function. Recently, reservoir computing has been implemented using MEMs devices with prevalent non-linear dynamics to perform non-linear processing tasks. While partially explored in the past, there has been renewed interest in using Surface Acoustic Wave devices as low energy radio-frequency processors. However they have yet to be explored in the reservoir computing framework. In this work, a 39.16 MHz two-port SAW resonator on chemically reduced YZ Lithium Niobate is design and measured. The quality factor, insertion loss, linear transmission, and non-linear transmission of the devices is measured, and the relationship of these properties to reservoir computing is discussed. The SAW resonator is then configured as a time-multiplexed reservoir, and it's non-linear processing capabilities are discussed using the time-delayed parity benchmark.

1 Introduction

The power consumed by neural networks is a major obstacle to the uptake of machine learning algorithms. This is true for both small- and large-scale applications. In small scale applications, the power and time requirements are prohibitive to cost effective implementation. However, even in the large scale, the time required for training means that real-time learning is often not feasible. In contrast, reservoir computing provides a compromise between training complexity and accuracy which facilitates real-time learning at both small and large scales. This can be achieved leaving the bulk of the neural network untrained, and only training the final layer of a traditional multilayer perceptron. Because the training is confined to a single layer, rather than spanning multiple layers with non-linear node activation, the complex and time consuming process of training by back propagation is reduced to a simple linear regression process. Conceptually this can visualised as separating the non-linear and linear processing components of a neural network into two separate networks in series.

Recently, the field of Physical reservoir computing has become more intensely researched. A Physical Reservoir Computer uses a physical system, like a MEMs transducer, actuator, or even an environmental system, as the neurons in a neural network. When a physical system is interconnected in a network-like manner, it allows the non-linear dynamics of the physical system to be used as a source of processing. A substantial problem for physical reservoir computers, and indeed many implementations of "neuromorphic" hardware, is the requirement for the nodes to be interconnected. When there are hundreds or thousands of nodes, it becomes impossible or impractical to interconnect them when using a planar fabrication technology (i.e. photo-lithographic processes).

As a result of this limitation, the "time delay" architecture has been conceived of. This structure was originally introduced for reservoir computing in 2011 (Larger et al. 2012), and since then many different physical reservoir computer implementations have been explored using it (Dion et al. 2018, Brunner et al. 2018, Duport et al. 2012, Duport et al. 2016).

A conceptual explanation of the time-delay neural network architecture is shown in Fig. 1. In this system, each input is multiplied by a time-domain series of weights, known as a masking function. Referring to the model of a multi-layer perceptron shown in Fig. 1, each value within the mask function corresponds to a single neuron in a hidden layer. The length of the mask function, N , then corresponds to the number of neurons per hidden layer.

✉ Claude Meffan
meffan.robertclaude.3i@kyoto-u.ac.jp

¹ Department of Microengineering, Kyoto University, Kyoto Daigaku-Katsura C3, Nishikyo-ku, Kyoto 615-8540, Japan

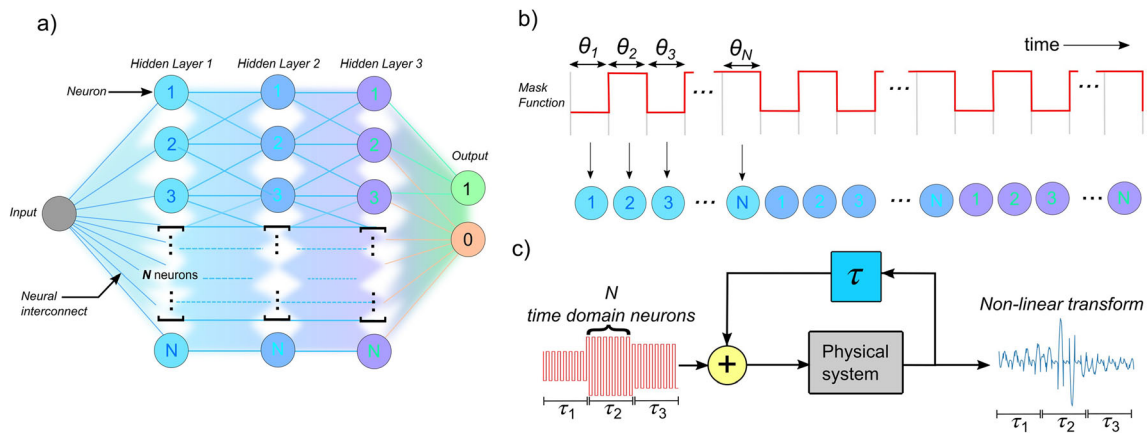


Fig. 1 A conceptual diagram of the time-delay architecture for creating a time-domain multiplexing of a multi-layered perceptron. **a** A conceptual model of the multi-layer perceptron. In this case, there are three hidden layers, and N neurons per hidden layer. **b** The usage of a mask function to create a time-domain hidden layer. Each input is multiplied with by a binary function of length N , creating a time

This transforms the hidden layer of a multi-layer perceptron into the time-domain, where each neuron is applied sequentially to a single physical neuron for a length of time θ . This creates a total hidden layer application time of $\tau = N\theta$.

For each time-domain neuron that is applied, the response of the system is then time-delayed by the total hidden layer application time τ , and then added back to the input of the system. As such, the re-input of the time-delayed response is synchronised with the corresponding neuron in the proceeding hidden layer. This time-delay process adds interconnection between subsequent hidden layers of the multi-layer perceptron.

Through these parameters, the coupling strength between neurons inside a single hidden layer, and between multiple hidden layers can be controlled through the rate that neurons are applied at, θ , as well as the attenuation that is applied to the time-delay input respectively.

In terms of implementation, while the masking function can be implemented by an arbitrary change to how transmitted data is encoded, the delay line is more difficult. In optical time-delay systems, the delay line is implemented through a length of fibre-optic cable. However, for most other physical reservoir computer systems, the delay line is not physically implemented, rather, the effect is simulated through traditional electronic memory and supporting apparatus.

In the past, and again more recently (Hackett et al. 2021), surface acoustic wave devices have been examined as radio frequency non-linear processors. In the past, these processors have been studied in the form of acoustic convolvers, parametric amplifiers, and frequency converters. In these devices cases, the non-linear parametric

domain hidden layer of N neurons. **c** A block diagram of the time-delay system. The time-domain hidden layer is applied, and then the response of the physical system is re-input after a time-delay. The length of the time-delay is such that each hidden layer neuron is coupled to the corresponding neuron in the subsequent hidden-layer

amplification effect is achieved through electrically coupling the SAW device with a non-linear transmission line (non-linear capacitors or inductors), or alternatively by using the non-linear compliance of the substrate material. Both these methodologies have been acknowledged to have limitations in the form large device areas required, or in the the strength of the non-linearity (and therefore power efficiency of non-linear processing), respectively. As a time-multiplexed neural network, however, other processes, such as the ring-down response of a resonator for example, may be used to as the non-linear neuronal activation function. As a result, an presently unexplored type of surface acoustic wave radio frequency processor may be possible in the form of the time-domain neural network reservoir computer. Additionally, SAW devices are well suited to time delay architecture. Surface waves have extremely low propagation loss for mechanical waves, and relatively long delaylines are readily fabricated. In addition, compared to optical implementations, devices can be 10^5 times smaller due to the lower phase velocity of mechanical waves. These combined factors could allow time-multiplexed recurrent neural networks of unprecedented size to be realised in a highly integrated form factor.

In this work, we present a proof-of-concept SAW reservoir computer using electronic memory to simulate a delay line. We measure the linear and nonlinear transmission properties of two-port SAW resonator devices and discuss their suitability for use in the time-multiplexed reservoir computer. Based on these results, we explore the parameter regions of high performance using the parity benchmark non-linear processing task.

2 Methods

The resonators in this work are two-port Rayleigh SAW resonators. The basic design of these resonators is shown in Fig. 2a. The resonator is composed of two distributed reflector structures, and two inter-digitated transducers (IDTs). The IDTs are placed between the two distributed reflector structures such that the distance between the reflectors creates a Fabry–Perot type resonant cavity. The resonant frequency of this structure is therefore determined by the overlap between the centre IDTs centre frequency, and the Fabry–Perot cavities resonances.

A detailed view of the IDTs and reflectors is shown in Fig. 2b. The center frequency, f_c , of the IDTs is,

$$f_c = p/v_{av} \tag{1}$$

where p is the electrode pitch, and the v_{av} is the average phase velocity of SAW waves in the structure. In this design, p is 87.2 μm , and v_{av} is 3410 ms^{-1} . This gives a center frequency of 39.16 MHz for the IDTs. Meanwhile, the Fabry–Perot cavity resonates when the spacing between the reflectors coincides with an integer number of wavelengths for a given frequency. In this design, the distance between the distributed reflectors is 25λ by design. As such the resonant cavity will also resonant at the IDTs centre frequency. The quality factor of two-port SAW resonators generally quite high, on the order of 10^4 (Campbell 2012). While in general a high quality factor is an attractive feature for a resonator, for time-domain reservoir computing applications, this property is more complicated. In a system such as this, the coupling between adjacent time-domain

neurons is controlled through the time-domain impulse response of the system (Brunner et al. 2018). As such, the strength of coupling between nodes is indirectly controlled through the quality factor, as well directly controlled through the neuron input rate, θ (Fig. 1b). For reservoir computers, or recurrent neural networks in general, it is desirable for networks to have so called “fading memory”. This property reflects the rate that the networks response to old inputs is retained, but gradually decays over time. This allows the network to perform non-linear processing with past inputs, but old/irrelevant inputs are forgotten in a timely manner.

Based on this requirement, it is desirable to control the quality factor the resonator node so that the time-domain response may be precisely controlled. The total loaded quality factor of the SAW resonator, Q_L , can be expressed in terms of the contributing losses parameters,

$$\frac{1}{Q_L} = \frac{1}{Q_m} + \frac{1}{Q_d} + \frac{1}{Q_b} + \frac{1}{Q_c} + \frac{1}{Q_e} \tag{2}$$

where Q_m is the material loss quality factor, Q_d is the diffraction related losses in the cavity and the reflectors, Q_b is losses due to conversion of SAW into bulk waves, Q_c is the efficiency of coupling to the external electrical circuit, and Q_e represents electrical losses due to resistance in the IDT fingers. Any of these loss mechanisms may be used to control the quality factor of the resonators. In this work, we examine Q_r in the distributed reflector structures as a method of quality factor adjustment. This method is advantageous because, as long as the Q_r losses are dominant, the quality factor can be controlled through the

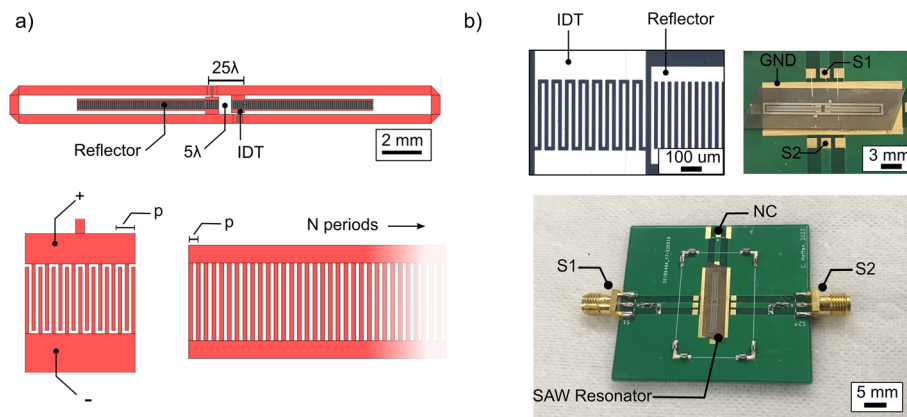


Fig. 2 The design and fabrication of the two-port SAW resonator. **a** An overview of the complete two-port SAW resonator design. The design consists of driving and transducing IDTs placed inside a resonant Fabry Perot cavity formed by two distributed reflectors. In this design, the acoustic cavity is 5 wavelengths wide and 25 wavelengths long. The IDT center frequency is 39.18 MHz, and 9 finger pairs, given a fractional bandwidth of 12.5%. **b** The fabricated SAW resonator mounted on top of the PCB measurement fixture. An optical micro-graph of the driving interdigitated transducer,

adjacent to the distributed Bragg reflector structure is shown on the top left. The top right photograph shows an image of the entire SAW resonator device mounted to the PCB. The edges of the device are angled so that stray SAW waves are scattered at the chip edge, and do not re-enter the resonant cavity. The bottom image shows the entire PCB measurement fixture. The board is configured as a non-insertable device for the measurement on a Vector Network Analyser. The interconnects include an L-shape matching networks, placed in-line with each port

number of strips (periods) in the distributed reflector i.e. photo-lithographically defined. However, Q_c is also of particular importance in analysing the performance of the RC system, as the devices properties will be influenced by the external electrical apparatus used to analyse a device.

2.1 Fabrication

The resonators were fabricated on chemically reduced YZ-LiNbO₃ (Yamaju Ceramics Co., Ltd.). Reduced Lithium Niobate was chosen for its large piezoelectric coupling coefficient of $K^2 = 0.045$, and reduced pyroelectric coefficient. The substrate was solvent cleaned (Acetone, Isopropyl Alcohol, and Deionized Water). They were then dehydrated on a hotplate at 150 °C for 10 min. AZ5214E image reversal photoresist (Microchemicals GmbH) is applied using a spin-coater (500 rpm, 10 s: 4000 rpm 30 s), followed by pre-baking at 110 °C for 50 s. The resist was exposed at 8.66 mJ.cm⁻² using a double sided mask aligner (Union PEM-800). An image reversal bake was then carried out at 117 °C for 2 min, followed by an additional, flood exposure, at 365 mJ.cm⁻². The wafer was developed in tetramethylammonium hydroxide for 36 s, followed by rinsing in deionized water. Using an electron-beam evaporator (custom made) 10 nm of chrome, followed by 100 nm of aluminium was deposited. Lift-off was then carried out in 80 °C N-Methyl-2-Pyrrolidone. The wafers were then diced into individual resonators using a dicing saw (Disco, DAD322) and glued onto a custom PCB with gold coated pads to facilitate wire-bonding.

2.2 Measurement

The linear response of the resonator was measured using the Pico106 Vector Network Analyzer (PicoVNA 106, Pico Technology Ltd). Before measurement, the vector network analyser was calibrated using a SOLT calibration standard (Standard 8.5 GHz SOLT calibration kit (SMA male), Pico Technology Ltd) to remove any contribution of the cabling and interconnects. The non-linear properties of SAW devices are conventionally assessed through the measurement of the either the single or two tone intermodulation distortion. In this case, a spectrum analyser (Rigol RS3015N, Rigol Technologies) was used to measure the single tone frequency spectrum of the resonator response relative to the input power spectrum.

2.3 Delay line reservoir

In future work, the delay line is intended to be replaced by a SAW delay line. However, in this work, the delay line functionality was implemented by using electronic memory. This allowed flexibility in the device configuration and

for a wide range of parameters to be examined. The masked data was input into the resonator through amplitude modulation, using an external frequency source with external modulation input (WF1968, NF Corporation). The magnitude and phase of the resonator response was measured using a lock-in amplifier (HF2LI, Zurich Instruments) which was phase locked to the sync output of the frequency source. A micro-controller system (CY8CKIT-050B Programmable System on a Chip, Infineon) was used to control the external modulation input, as well act as the delay line. A PSoC type device was chosen as it's reconfigurable analog co-processor and direct-memory-access controller allows for low latency operation.

In the micro-controller system, a re-configurable PWM timer was used to time the inputs of time-domain neurons. The PWM interrupt line was physically connected to the start-of-conversion pin of the ADC using the PSoCs dynamically reconfigurable interconnect layer. The ADCs end-of-conversion pin directly triggered the direct memory access (DMA) controller to transfer the result out of ADC memory and into a circular buffer array. This circular buffer acts as the delay line. The DMA controllers transaction descriptor is configured to reset after N data transfers have occurred, where N is the length of the masking function (equivalently, the number of time domain neurons per hidden layer). This resets the direct-memory access controller, allowing it to act as a looping/circular function also. The values of the resonators response was recorded by a PC connected via USB to the lock-in amplifier. The maximum rate of the internal data server is 500 kHz. As such the theoretical minimum time domain neuronal spacing, θ , is 1–2 μ s. However, practically the limitation is 20 μ s. After the experiment is completed, the recorded data is in the form of a single vector of length $n \times N$. Where N is the number of Nodes in a hidden layer and n and is the number of inputs applied. This can be reshaped into an $n \times N$ matrix, which essentially gives the neuron responses for each input. A reservoir computer does not train all weights and activations of the individual neurons, and instead uses a modified linear regression using the neuron values. In this work, a linear regression with Tikhonov regularisation (also known as a Ridge Regression) was used to fit the $n - X$ observations of the N neurons to a pre-calculated stream of parity values (used as training data). X is the number of inputs used to test the performance of the system. After the fitting process, the output of the reservoir computer for the remaining X inputs can compared to the correct value to calculate the success rate of the system.

Further detail on this process can be found in literature (Brunner et al. October 2018).

2.4 Reservoir computing task

There are many different reservoir computing tasks which are used to test different implementations. Common examples include non-linear channel estimation (Paquot et al. 2012; Jaeger 2004; Paquot et al. 2012), waveform classification (Tanaka et al. 2017), speech recognition (Araujo et al. 2020; Dion et al. October 2018; Paquot et al. 2012), time-series prediction tasks (Soriano et al. 2013), and the time-delay binary parity task (Dion et al. 2018). In this work, we examine the time-delay binary parity task due to its simple definition and ability to quickly and simply generate a new dataset. This benchmark task is popular in reservoir computing research as it evaluates both the memory, and the non-linear processing capability of a recurrent neural network. The time-delayed parity function, $P_{n,\delta}(t)$ as a function of time can be defined as,

$$P_{n,\delta}(t) = \prod_{i=0}^{n-1} u [t - (i + \delta)]T \tag{3}$$

In this case, binary information, encoded as levels of $(1, -1)$, is input at a rate of τ^{-1} , t is time, δ is the time delay, and n is the order of the parity task (how many bits are considered in the parity calculation). The parity function is a Boolean function which returns either true (1) or false (-1) if the number of high inputs in a certain range is even or odd numbered. In contrast, the time-delayed parity task performs this same calculation, but considers inputs δ time steps into the past. Although conceptually simple, this task is quite challenging, and tests both the memory capacity, and the non-linear processing capacity of the time-domain neural network.

3 Results

Figure 2b shows the fabricated SAW resonator structure. The devices were diced from the wafer in a non-rectangular grid. The non-rectangular dicing grid allowed for stray SAW waves to be scattered by the edges of the chips, meaning that wave absorption materials at the edges of the chip were unnecessary. The devices were operated in atmospheric pressure, with a plastic protective covering to protect the devices during handling. Following mounting on the measurement fixture, the 2 port s-parameters of SAW resonators was measured using the vector network analyser. Figure 3a shows this measurement for devices with varying distributed reflector periods (and therefore reflectivity).

As a result of the varied losses in the distributed reflector structures, the quality factor of the resonators varied from 400 at the lowest to 1600 at the highest. The relationship

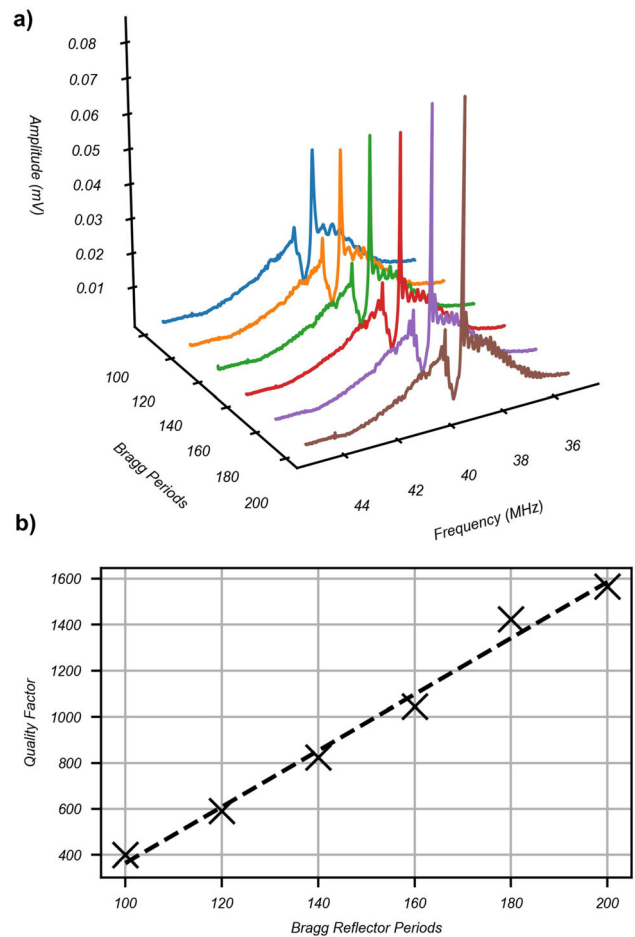


Fig. 3 The linear transmission properties of a range of 2-port SAW resonator. **a** The linear transmission spectrum of the SAW resonator. The quality factor of the resonator can be effectively adjusted through the reflectivity of the distributed reflectors surrounding the resonant cavity. **b** The quality factor of the resonator as a function of metal strips in the distributed reflectors

between decreasing losses in the reflector structures, and increase in quality factor is shown in Fig. 3b. Each data point represents multiple measurements of selected singular samples from the wafer. There was moderate variation between samples on the wafer, however this appeared to be due to variation in packaging methods (electrically limited Q factor). In the future, the packaging of the devices will need to be improved so that the quality factor of the resonators can be precisely engineered, and tailored using lithographically or electrically defined means. For the purposes of this work, we simply select the sample which has the appropriate quality factor value.

With respect to physical reservoir computing, controlling the quality factor is useful as it allows the strength of time-domain neuron coupling to be controlled through physical design parameters. In time-multiplexed neural networks, such as this system, there is an optimal neuron input rate θ in which neurons are sufficiently coupled to

provide memory and non-linearity, but still inside the bandwidth of the physical system. As such, the optimal value of θ is related to the characteristic time of the system, T . Relative to the characteristic time, the optimum neuron input time can vary substantially depending on the physical system (Appeltant et al. 2011; Dion et al. October 2018).

3.1 Reservoir computing performance

With respect to the resonators tested in Fig. 3 we select the quality factor 1600 resonator to test as a reservoir computer. Due to the 500 kHz maximum data rate of the lock-in amplifiers internal data server, the practical experimental limit for θ values is approximately 20 μ s. Although this is still substantially larger than characteristic time of the system, some meaningful performance may still be obtained. The mask function in this experiment is a binary maximum length set (Alpeltant et al. 2014) of length 127. This creates 127 virtual nodes in the hidden layers of the reservoir. The gain for the output IDT prior to the delay line was 3. For the time delayed binary parity task, 1200 randomly generated inputs were fed into the reservoir in the manner described in Sect. 1. The first 1000 inputs were used to train the output layer (see Fig. 1), while the final 200 inputs were used to evaluate the performance of the system.

The performance of the reservoir computer for parity order 2–7, but zero delay ($\delta = 0$), is shown in Fig. 4. Figure 4a shows a heat-map of parity success-rate as a function of both driving frequency and node-input rate, θ . This shows that for low order, P2 and P3 tasks, the high performance area is wide, and is not strongly influenced by

the resonators response. However, as the parity task becomes more difficult (Parity Order 4–7) then the region of higher performance becomes smaller, and is confined within the bandwidth of the resonant cavity. Figure 4b shows the real-time output of the reservoir computer alongside the actual parity stream. The output of the reservoir in this case, represents the certainty of the reservoir in the output value. As a result, when the reservoirs output is thresholded—there is good performance even for high order tasks (95% for Parity order 5, 82% for Parity Order 6). However due to the increased uncertainty of the output, there is a higher bit-error rate.

Beyond the simple parity success rate, for a more comprehensive evaluation of the reservoir computers performance, the mutual information, MI , and memory capacity, MC can be calculated (Hou et al. 2018). The mutual information for the time-delayed binary parity task can be defined as,

$$MI_{n,\delta} = p_{n,\delta} \log_2(2p_{n,\delta}) + (1 - p_{n,\delta}) \log(2(p_{n,\delta})) \quad (4)$$

where $p_{n,\delta}$ the success rate of the reservoir computer in predicting the time delayed parity task of a particular order and delay time. Meanwhile, the memory capacity of the reservoir is,

$$MC_n = \sum_{\delta=0}^{\infty} MI_{n,\delta} \quad (5)$$

Both of these quantities are measured in Shannon information content, or Bits (MacKay et al. 2003). The mutual information is the Shannon information content in the reservoir regarding one specific parity task with an order n , and delay-time δ . In contrast, the memory capacity

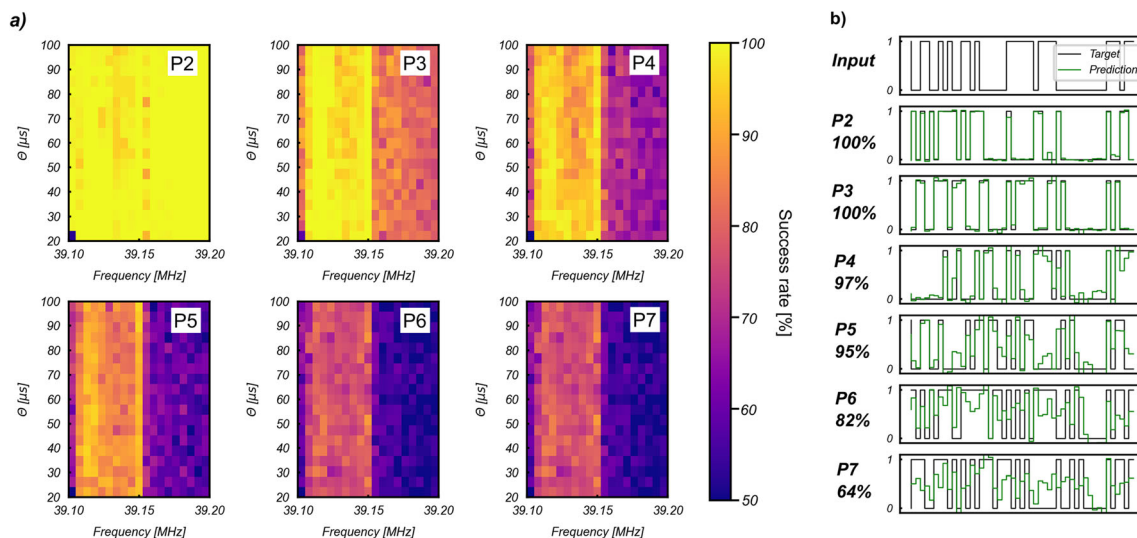


Fig. 4 The performance of the Surface acoustic wave reservoir computer on the Parity benchmark task. **a** The performance of the delay-line reservoir computer on various order parity tasks. Each

experiment is shown as a function of driving frequency and node-input rate, θ . **b** The target parity stream alongside the prediction of the reservoir computer

is the total Shannon information content contained within the reservoir about a parity task of order n , for all time-delay values. Compared to the simple success rate, the memory capacity shows the areas where the reservoir contains the largest information content about the task. Figure 5a shows a plot of the resonance frequency over the narrow bandwidth of the Fabry–Perot cavities resonant peak. As mentioned previously, the quality factor and resonance frequency is effected by the external electrical circuitry—as such the resonance frequency and quality factor shown in Fig. 3 a) is different to that measured by the lock-in amplifier in-situ. When connected into the delay line circuit, the measured resonant frequency is shifted by

$\sim 0.01\%$ to 39.139 MHz, and the quality factor reduced substantially. Figure 5b shows the memory capacity of the reservoir for the parity order 2 task as a function of driving frequency and neuron input rate, θ . The memory capacity is the sum of all the mutual information, or information content, for the order 2 parity task between 0, and 8 delay time-steps. Above 8 delay steps, the reservoir contained no information content, and therefore the summation was truncated at 8 delay steps. The information content in the reservoir for various order parity tasks is shown in Fig. 5c. The maximum memory of the reservoir is 4.79 bits for the order 1 parity task. For a virtual neural network of width 127 neurons, this is near equivalent or improved performance, to other computers in literature (Dion et al. 2018).

The high performance areas of the reservoir can be found by examining the areas of high memory capacity in Fig. 5b. Interestingly, the high performance areas are concentrated to either side, but not exactly on, the resonant peak of the system. Initially it was hypothesized that this may align with the lower and upper side bands of of the AM modulated input signal. However, the side bands do not appear to align with this. The upper and lower AM side bands are indicated in Fig. 5b as dashed lines.

4 Discussion

For a recurrent neural network, a non-linear neuron activation functions, as well as memory/interconnection are generally required (Dion et al. 2018). As already discussed, in this system, the interconnection aspect of this is provided using the time-delay multiplexed neural network. With regards to the nonlinear activation function, in other physical reservoir computer systems, the non-linear activation function is generally considered to be some source of non-linearity in the governing dynamics of the MEMS system. For example, spring-hardening/softening effects in silicon resonators (Dion et al. 2018; Barazani et al. 2020), or sinusoidal actuation curves of optical modulators (Dupont et al. 2012; Larger et al. 2012).

For the SAW device in this work, either the ring-down response, or the intermodulation distortion resulting from the non-linear compliance of the substrate material was expected to act as the non-linear neuron activation function. It was suspected that the exponential curve of the ring-down response could act as the non-linear activation function, as is this has been reported in other studies (Sun et al. 2021). However, due to limitations in the delay line experimental apparatus, the time domain neuron input rates is theoretically much larger then the optimal input rate for use of this non-linear response. When examining the time domain response of the system when configured as in the delay loop (not shown), it appears that the resonators

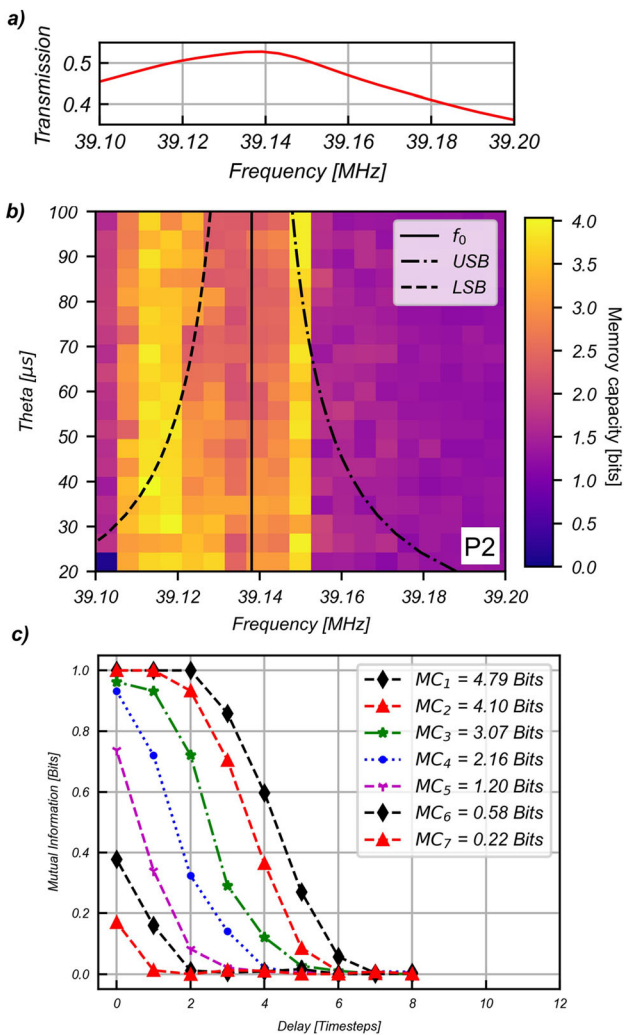


Fig. 5 The memory capacity of the reservoir computer when performing the time delayed binary parity task. **a** The memory capacity of the reservoir computer as a function of driving frequency and virtual node spacing θ . **b** The mutual information of the reservoir as a function of task delay line. As the complexity of the task increases, the mutual information decreases. Signifying that the information needed to complete the task is not contained within the reservoir

transient response has finished within one time-domain neuron. As such it should not be a contributor to the non-linear activation of a neuron.

An alternative strategy, which has been used in past attempts to create non-linear SAW processors is using the non-linear compliance of the substrate material (Luukkala and Kino 1971; Robbins 1975; Schneider et al. 2020). This non-linear compliance produces intermodulation distortion of signals within a SAW system. While it is considered to be a small second-order effect, in the past, power compressing structures and low aperture IDTs have been used to make SAW devices with non-linear processing capability. In this work, the IDTs are designed with a small 5λ aperture. This applies the electrical power over a small acoustic cross-section. For lithium niobate, the threshold for linear operation is considered to be approximately 10 mW/mm of acoustic aperture (Campbell 2012). The radiation conductance of the IDTs was calculated using the cross-field model (Campbell 2012). The radiation conductance of the driving and sensing IDTs was 0.588 mS . As such, there should be significant non-linear operation at above $\sim 2.7\text{ V}$. The single tone intermodulation distortion was used to verify this, through measuring the frequency spectrum of the resonators single tone response. This is shown in Fig. 6a. In this case, the generated 2nd harmonic frequency at $\sim 78.2\text{ MHz}$ can be observed in the frequency response spectrum. However, there is also substantial third order intermodulation products apparent in the driving signal. The resonators S_{12} transmission at 78 MHz was measured to be -69 dB using the vector network analyser. The second harmonic signal experiences only -44 dB of attenuation. As such the response is ~ 20 times larger than the linear transmission measurements predict. Despite this, the single tone intermodulation distortion is very small, and the device essentially appears to be operating linearly. Based on these measurements, it is hypothesised that the non-linear activation function is provided by the coupling of higher order intermodulation products into the resonant cavity. This may why the high memory areas of the reservoir cluster at the edges of the resonant peak, rather than at the resonant peak. However, more work needs to be done to validate this hypothesis.

For the purposes of a reservoir computer, it is often stated that such systems function best when driven “at the edge of chaos” (Schurmann et al. 2004). Although this statement is often debated (Carroll 2020), it generally hints at the requirement for a strongly non-linear system, which is capable of chaotic dynamics. For systems with substantially non-linear dynamics, the intensity that the system is driven often plays a determining role in what kind of dynamic behaviour is observed (Strogatz 2019). To examine the role of driving amplitude on the performance of the reservoir in this work, the driving amplitude of the

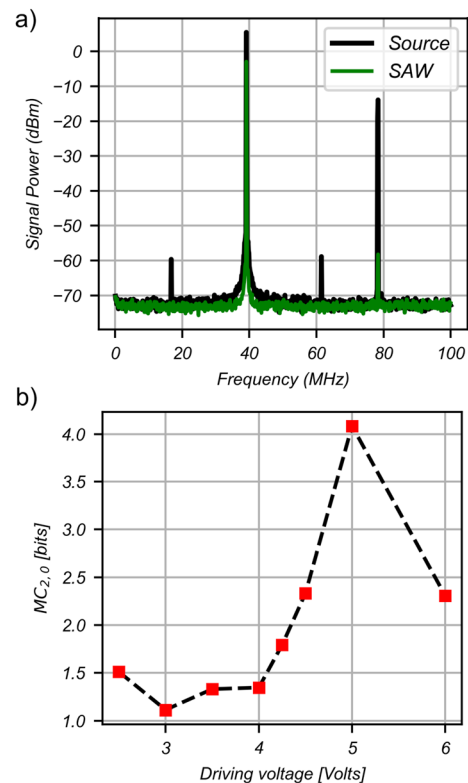


Fig. 6 Investigation into the source of non-linear activation function of the reservoir computer. **a** Intermodulation distortion inside the SAW resonator. The magnitude of the intermodulation distortion is much larger than otherwise predicted by the linear transmission measurements. **b** Memory Capacity of the reservoir computer as a function of driving voltage. Above 4 V there is a sudden increase in memory capacity. Above 5 V the memory capacity suddenly decreases

modulated signal driving the resonator was varied, and the memory capacity calculated for each driving amplitude. Here, the driving frequency was 39.11 MHz and the time domain neuron input rate was $40\text{ }\mu\text{s}$. These values coincide with the highest performance parameters as shown in Fig. 5b.

For lithium niobate, the threshold for non-linear behaviour is reached at approximately 10 mW/mm of acoustic aperture (Campbell 2012). It is hypothesized that driving powers beneath this level would not function well. Indeed, Fig. 6b shows that for driving voltages or powers beneath 4 V have a comparatively small amount of information content ($1.0\text{--}1.5\text{ bits}$). However, above 4 V the information content of the reservoir increases dramatically up to more than 4 Bits . When driven over 5 V , the memory capacity of the reservoir dramatically decreases again. The decrease in memory capacity at higher driving voltages might be attributed to the already mentioned “edge of chaos” theory for reservoir computing, however chaotic dynamics could not be confirmed in the resonator. Further investigation is warranted in this matter.

In the future, we wish to further study the source of non-linear activation in the SAW resonator reservoir computer. In addition, the device will be integrated with a physical SAW delay-line to create a fully integrated surface acoustic wave reservoir computer.

5 Conclusion

Here we report the first example of a piezoelectric surface acoustic wave reservoir computer. The system utilised a two-port SAW resonator device, and an electronic delay line apparatus, to create a time-multiplexed recurrent neural network. The system was shown to perform the parity task non-linear processing benchmark with comparable performance to literature reservoir computers. Using SAW resonator devices is advantages for physical reservoir computing systems due to the ability for the system to be integrated with a SAW delay line structure. As such there is potential to create a fully integrated physical reservoir computer. Such systems could have performance comparable to optical implementations, however with the capability for a physical size 10^5 times smaller than the optical counterpart.

In the future, we wish to study the non-linear activation function for timedomain neurons in the system to further understand the operation. In addition, we wish to integrate the resonator structure with the well established piezoelectric SAW delay line to create a fully-integrated micro-mechanical reservoir computer system.

Acknowledgements This work is supported by the Japan Society for the Promotion of Science (JSPS) Grants-in-Aid for Scientific Research JSPS KAK-ENHI Grant Number 21F20799 and 22K18289, Tateisi Science and Technology Foundation, and the Telecommunications Advancement Foundation. We also acknowledge technical support from Kyoto University Nanotechnology Hub in the “ARIM Project” sponsored by MEXT, Japan (JPMXP12-22KT1250).

Data availability The data generated for use in this paper is available online: <https://doi.org/10.5281/zenodo.7939299>.

References

- Appeltant L, Soriano MC, Van der Sande G, Danckaert J, Massar S, Dambre J, Schrauwen B, Mirasso CR, Fischer I (2011) Information processing using a single dynamical node as complex system. *Nat Commun* 2(1):468
- Appeltant L, Van der Sande G, Danckaert J, Fischer I (2014) Constructing optimized binary masks for reservoir computing with delay systems. *Sci Rep* 4(1):3629
- Araujo FA, Riou M, Torrejon J, Tsunegi S, Querlioz D, Yakushiji K, Fukushima A, Kubota H, Yuasa S, Stiles MD, Grollier J (2020) Role of non-linear data processing on speech recognition task in the framework of reservoir computing. *Sci Rep* 10(1):328

- Barazani B, Dion G, Morissette JF, Beaudoin L, Sylvestre J (2020) Microfabricated neuroaccelerometer: integrating sensing and reservoir computing in MEMS. *J Microelectromech Syst* 29(3):338–347
- Brunner D, Penkovsky B, Marquez BA, Jacquot M, Fischer I, Larger L (2018) Tutorial: Photonic neural networks in delay systems. *J Appl Phys* 124(15):152004
- Colin Campbell. 2012 Surface Acoustic Wave Devices and Their Signal Processing Applications.
- Carroll TL (2020) Do reservoir computers work best at the edge of chaos? *Chaos Interdiscip* 30(12):121109
- Dion G, Mejaouri S, Sylvestre J (2018) Reservoir computing with a single delay-coupled non-linear mechanical oscillator. *J Appl Phys* 124(15):152132
- Duport F, Schneider B, Smerieri A, Haelterman M, Massar S (2012) All-optical reservoir computing. *Opt Express* 20(20):22783
- Duport F, Smerieri A, Akrouf A, Haelterman M, Massar S (2016) Fully analogue photonic reservoir computer. *Sci Rep* 6(1):22381
- Hackett L, Miller M, Brimigion F, Dominguez D, Peake G, Tauke-Pedretti A, Arterburn S, Friedmann TA, Eichenfield M (2021) Towards single-chip radiofrequency signal processing via acoustoelectric electron-phonon interactions. *Nat Commun* 12(1):2769
- Hou Y, Xia G, Yang W, Wang D, Jayaprasath E, Jiang Z, ChunXia H, ZhengMao W (2018) Prediction performance of reservoir computing system based on a semiconductor laser subject to double optical feedback and optical injection. *Opt Express* 26(8):10211–10219
- Jaeger H (2004) Harnessing nonlinearity: predicting chaotic systems and saving energy in wireless communication. *Science* 304(5667):78–80
- Larger L, Soriano MC, Brunner D, Appeltant L, Gutierrez JM, Pesquera L, Mirasso CR, Fischer I (2012) Photonic information processing beyond turing: an optoelectronic implementation of reservoir computing. *Opt Express* 20(3):3241–3249
- Luukkala M, Kino GS (1971) Convolution and time inversion using parametric interactions of acoustic surface waves. *Appl Phys Lett* 18(9):393–394
- MacKay DJC, Mac Kay DJC (2003) Information Theory, Inference and Learning Algorithms. Cambridge University Press
- Paquot Y, Duport F, Smerieri A, Dambre J, Schrauwen B, Haelterman M, Massar S (2012) Optoelectronic reservoir computing. *Sci Rep* 2(1):287
- Robbins WP (1975) Pump requirements for parametric amplification and generation of surface waves on YZ LiNbO₃. *IEEE Trans Son Ultrason* 22(4):257–263
- Schneider JD, Ting L, Tiwari S, Zou X, Mal A, Candler RN, Wang YE, Carman GP (2020) Frequency conversion through nonlinear mixing in acoustic waves. *J Appl Phys* 128(6):064105
- Schürmann F, Karlheinz M, and Schemmel J. Edge of Chaos Computation in Mixed-Mode VLSI - A Hard Liquid. In *Advances in Neural Information Processing Systems*, volume 17. MIT Press, 2004
- Soriano MC, Ortín S, Brunner D, Larger L, Mirasso CR, Fischer I, Pesquera L (2013) Optoelectronic reservoir computing: tackling noise-induced performance degradation. *Opt Express* 21(1):12–20
- Strogatz SH (2019) Nonlinear dynamics and chaos: with applications to physics, biology, chemistry, and engineering, 2nd edn. CRC Press, Boca Raton
- Sun J, Yang W, Zheng T, Xiong X, Liu Y, Wang Z, Li Z, Zou X (2021) Novel nondelay-based reservoir computing with a single micromechanical nonlinear resonator for high-efficiency information processing. *Microsyst Nanoeng* 7(1):1–11
- Tanaka G, Nakane R, Yamane T, Takeda S, Nakano D, Nakagawa S, Hirose A (2017) Waveform classification by memristive

reservoir computing. In: Liu D, Xie S, Li Y, Zhao D, El-Alfy E-S (eds) Neural information processing. Springer International Publishing, Cham, pp 457–465

Publisher's Note Springer Nature remains neutral with regard to jurisdictional claims in published maps and institutional affiliations.

Springer Nature or its licensor (e.g. a society or other partner) holds exclusive rights to this article under a publishing agreement with the author(s) or other rightsholder(s); author self-archiving of the accepted manuscript version of this article is solely governed by the terms of such publishing agreement and applicable law.